

Article

Advanced MPPT Algorithm for Distributed Photovoltaic Systems

Hyeon-Seok Lee ¹  and Jae-Jung Yun ^{2,*}

¹ Department of Electrical Engineering, POSTECH, Pohang 37673, Korea; hsaadf@postech.ac.kr

² Department of Electronics and Electrical Engineering, Daegu University, Gyeongsan 38453, Korea

* Correspondence: jjyun@daegu.ac.kr; Tel.: +82-53-850-6612

Received: 22 August 2019; Accepted: 18 September 2019; Published: 19 September 2019



Abstract: The basic and adaptive maximum power point tracking algorithms have been studied for distributed photovoltaic systems to maximize the energy production of a photovoltaic (PV) module. However, the basic maximum power point tracking algorithms using a fixed step size, such as perturb and observe and incremental conductance, suffer from a trade-off between tracking accuracy and tracking speed. Although the adaptive maximum power point tracking algorithms using a variable step size improve the maximum power point tracking efficiency and dynamic response of the basic algorithms, these algorithms still have the oscillations at the maximum power point, because the variable step size is sensitive to external factors. Therefore, this paper proposes an enhanced maximum power point tracking algorithm that can have fast dynamic response, low oscillations, and high maximum power point tracking efficiency. To achieve these advantages, the proposed maximum power point tracking algorithm uses two methods that can apply the optimal step size to each operating range. In the operating range near the maximum power point, a small fixed step size is used to minimize the oscillations at the maximum power point. In contrast, in the operating range far from the maximum power point, a variable step size proportional to the slope of the power-voltage curve of PV module is used to achieve fast tracking speed under dynamic weather conditions. As a result, the proposed algorithm can achieve higher maximum power point tracking efficiency, faster dynamic response, and lower oscillations than the basic and adaptive algorithms. The theoretical analysis and performance of the proposed algorithm were verified by experimental results. In addition, the comparative experimental results of the proposed algorithm with the other maximum power point tracking algorithms show the superiority of the proposed algorithm.

Keywords: PV system; P&O; INC; adaptive; DC–DC converter; DMPPT

1. Introduction

The renewable energy resources including wind power, biomass, solar heating, solar photovoltaic (PV), hydroelectric energy, and fuel cells have been widely used to reduce global warming effects caused by greenhouse gas emission [1–4]. Among these energy resources, solar PV has attracted attention as a promising renewable energy source due to the following reasons:

1. Diverse applications: PV system can be easily applied to microgrid, households, and buildings [5–7].
2. Low maintenance costs: Only PV module, inverter, and cable are required for maintenance and the maintenance period is long [8–10].
3. Technology development: Various methods were constantly introduced to improve the technology in the solar power industry [8–10].

PV systems consist of PV modules for converting sunlight into direct current (DC) electricity, as well as PV inverters for converting DC into alternating current (AC). Based on the connection

method between the PV module and the PV inverter, the PV inverter can be categorized as a central inverter or as a module-level power electronic (MLPE). In the past, central inverters (Figure 1a) connected with series-connected PV modules were widely used because they have the advantages of simple structure and low cost [11]. However, central inverters suffered from significant performance degradation under partial shading due to multiple maximum power points and mismatches in PV modules. To solve the partial shading problem, MLPEs (Figure 1b), which include a DC-optimizer and a micro-inverter, were introduced [12–16]. MLPEs are connected to one PV module and harvest optimum power by performing module-level maximum power point tracking (MPPT); this is also known as distributed MPPT (DMPPT) [17–19]. Thereby, MLPEs solve the partial shading problem and improve the performance of an entire PV system.

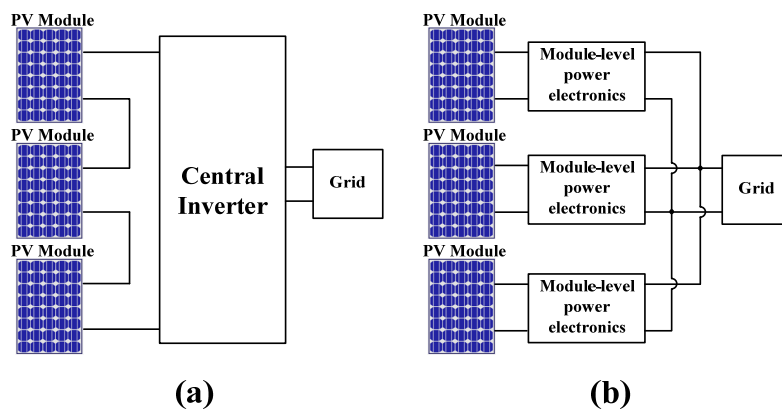


Figure 1. Block diagrams of (a) the central inverter and (b) the module-level power electronics.

Among many MPPT algorithms, hill-climbing, perturb and observe (P&O), and incremental conductance (INC) have been widely used due to their simplicity and ease of implementation [20–24].

Hill-climbing and P&O algorithms operate on the same fundamental principle that the variation (ΔV_{PV}) of PV voltage (V_{PV}) and the variation (ΔP_{PV}) of PV power (P_{PV}) become zero at the maximum power point (MPP). The difference between the P&O and hill-climbing algorithms is that P&O uses a PI controller. Operations in both hill-climbing and P&O algorithms can be classified into five modes and are described in Figure 2 and Table 1 [20–23]. The INC algorithm tracks the MPP based on the principle that the variation (ΔI_{PV}) of PV current (I_{PV}) becomes zero and the slope of $-\Delta I_{PV}/\Delta V_{PV}$ is the same as I_{PV}/V_{PV} at the MPP. The INC algorithm also has five operating modes, and its principle of operation is described in Figure 3 and Table 2 [24]. However, these basic MPPT algorithms have a trade-off problem between tracking accuracy and speed because fixed step size is used for perturbation. If small fixed step size is used, tracking accuracy increases, but speed is slower. In this case, the basic MPPT algorithms can fail to track the MPP under dynamic weather conditions. At large fixed step size, tracking speed is faster, but tracking accuracy decreases, which causes a low MPPT efficiency.

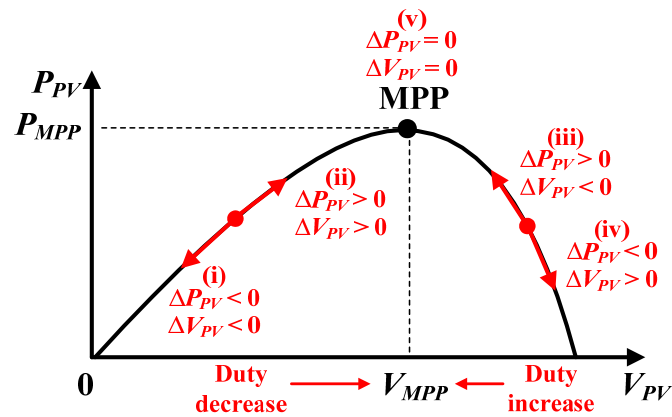


Figure 2. Principle of operation for the hill-climbing and perturb and observe (P&O) algorithms.

Table 1. Methodology of the hill-climbing and P&O algorithms.

Conditions	Actions
(i) $\Delta P_{PV} < 0$ and $\Delta V_{PV} < 0$	Duty decrease
(ii) $\Delta P_{PV} > 0$ and $\Delta V_{PV} > 0$	Duty decrease
(iii) $\Delta P_{PV} > 0$ and $\Delta V_{PV} < 0$	Duty increase
(iv) $\Delta P_{PV} < 0$ and $\Delta V_{PV} > 0$	Duty increase
(v) $\Delta P_{PV} = 0$ and $\Delta V_{PV} = 0$	No action

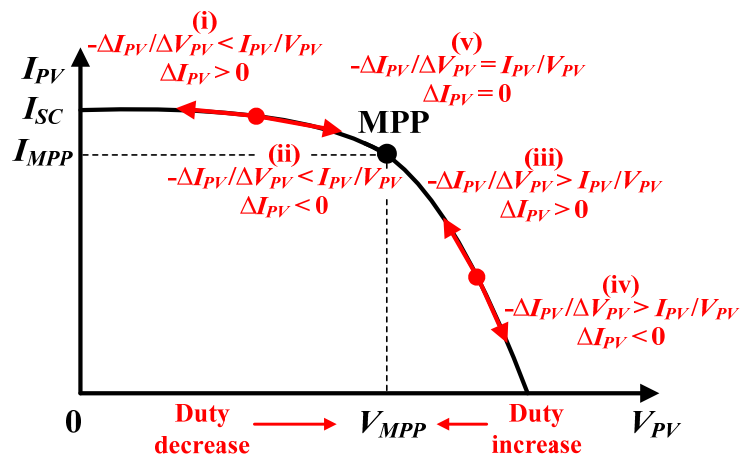


Figure 3. Principle of operation for the incremental conductance (INC) algorithm.

Table 2. Methodology of the INC algorithm.

Conditions	Actions
(i) $-\Delta I_{PV}/\Delta V_{PV} < I_{PV}/V_{PV}$ and $\Delta I_{PV} > 0$	Duty decrease
(ii) $-\Delta I_{PV}/\Delta V_{PV} < I_{PV}/V_{PV}$ and $\Delta I_{PV} < 0$	Duty decrease
(iii) $-\Delta I_{PV}/\Delta V_{PV} > I_{PV}/V_{PV}$ and $\Delta I_{PV} > 0$	Duty increase
(iv) $-\Delta I_{PV}/\Delta V_{PV} > I_{PV}/V_{PV}$ and $\Delta I_{PV} < 0$	Duty increase
(v) $-\Delta I_{PV}/\Delta V_{PV} = I_{PV}/V_{PV}$ and $\Delta I_{PV} = 0$	No action

To solve these problems, adaptive hill-climbing, adaptive P&O, and adaptive INC algorithms using variable step sizes were introduced [25–28]. In each adaptive MPPT algorithm, a variable step size is automatically adjusted according to the slope formula consisting of the variations (ΔP_{PV} and ΔV_{PV}) and variable step coefficients (a , N , and M); $a \cdot \Delta P_{PV}/\Delta V_{PV}$ in [25,26], $N \cdot \Delta P_{PV}/\Delta V_{PV}$ in [27], and $M \cdot \Delta P_{PV}/\Delta V_{PV}$ in [28]. The variable step size becomes high far from the MPP and low near the MPP. Therefore, the adaptive MPPT algorithms can achieve fast tracking speed in the operating range far

from the MPP and small oscillations in the operating range near the MPP. However, these algorithms still have oscillations at the MPP because the variables (ΔP_{PV} and ΔV_{PV}) in the slope formula are easily affected by sensing and calculation errors, sensing noise, and ripples of V_{PV} and I_{PV} .

In [29–32], the MPPT algorithms with intelligent prediction were introduced. Some of the algorithms used fuzzy logic to vary the step size [29–31]; the fuzzy logic method consists of fuzzification, a fuzzy rule-based lookup table (Table 3), and defuzzification. First, the input variables (ΔI_{PV} and ΔP_{PV}) are converted into fuzzy subsets such as negative big (NB), negative small (NS), zero (ZO), positive small (PS), and positive big (PB) depending on ΔI_{PV} and ΔP_{PV} . Then, one fuzzy subset is determined based on the rule-based lookup table and it provides a numeric step size. The MPPT algorithm using fuzzy logic is effective in dealing with the nonlinear characteristics of the PV module because the fuzzy logic divides the nonlinear system in the fuzzy subsets defined by the variables (ΔI_{PV} and ΔP_{PV}) and controls the nonlinearity of system using the rule base for each area (See Table 3). Therefore, it can track the MPP well under dynamic weather conditions. However, compared to other MPPT algorithms such as adaptive P&O and INC algorithms, it requires a digital signal processor (DSP) with higher specification and also makes the user's design more difficult because of its higher complexity of algorithm and execution process [27,31]. This is a disadvantage for commercialization. The other MPPT algorithm of [32] changed the step size by using a PID controller tuned by genetic algorithm. First, the genetic algorithm evaluates a number of solutions known as chromosomes using a fitness function, and later, genetic operators (selection, crossover, and mutation) are applied until a stop criterion is satisfied (Figure 4). Based on this principle of the genetic algorithm, the PID coefficients (K_p , K_i , and K_d) are determined to vary the step size. This MPPT algorithm also has good performance under dynamic weather conditions, but it requires high computational capability and sophisticated controllers due to its complexity.

Table 3. Rule-based lookup table based on the fuzzy logic.

ΔI_{PV}	ΔP_{PV}				
	NB	NS	ZO	PS	PB
NB	NB	NS	NS	ZO	ZO
NS	NS	ZO	ZO	ZO	PS
ZO	ZO	ZO	ZO	PS	PS
PS	ZO	PS	PS	PS	PB
PB	PS	PS	PB	PB	PB

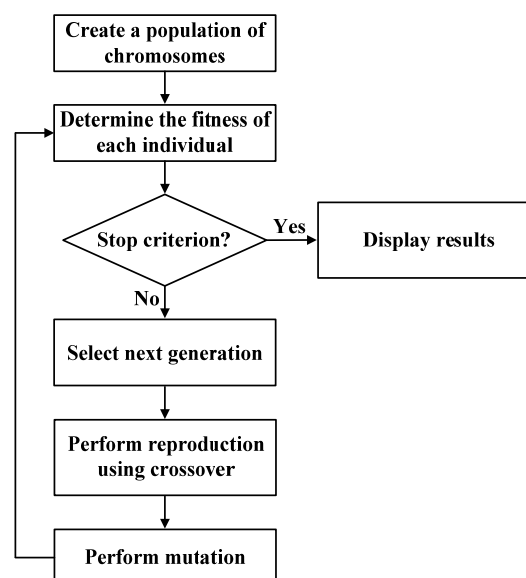


Figure 4. Flow chart of the genetic algorithm.

In this paper, an advanced MPPT algorithm for DMPPT in the MLPEs is proposed, which improves the tracking speed and accuracy under both steady and dynamic weather conditions. Similar to the adaptive MPPT algorithms, the proposed MPPT algorithm automatically changes the variable step size according to the slope of $\Delta P_{PV}/\Delta V_{PV}$ in the operating range far from the MPP. However, in the operating range near the MPP, it accurately tracks the MPP using a small fixed step size. As a result, the proposed MPPT algorithm achieves small oscillations at the MPP and a fast dynamic response. In addition, compared with the MPPT algorithms with intelligent control such as fuzzy logic and PID, the proposed MPPT algorithm can reduce the computational load of DSP because it is based on simple P&O method. Therefore, it allows manufacturers to use cheap DSPs for the PV system.

The distributed PV system and proposed MPPT algorithm are described in Section 2, the experimental results and discussion are presented in Section 3, and a conclusion is given in Section 4.

2. Distributed PV System and Proposed MPPT Algorithm

2.1. Distributed PV System

A distributed PV system with the MPPT algorithm is shown in Figure 5; the system consists of one PV module and one MLPE. Due to the fact that the PV module converts sunlight into low DC voltage, the MLPE requires a high voltage gain to convert low DC voltage into high AC voltage with grid frequency. The MPPT algorithm controls the duty ratio (D) of the MLPE to operate at the MPP of the PV module. To perform the MPPT algorithm, the voltage (V_{PV}) and current (I_{PV}) of the PV module are used as input signals.

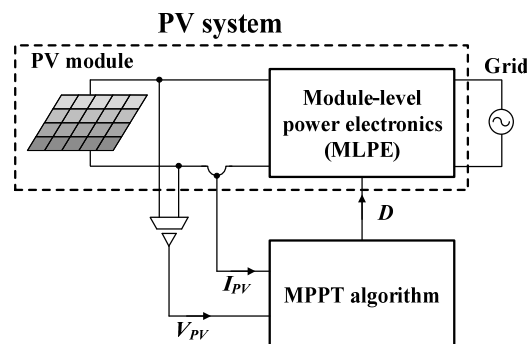


Figure 5. Diagram of the distributed photovoltaic (PV) system with maximum power point tracking (MPPT) algorithm.

2.1.1. PV Module

Based on the references [33,34], the equivalent circuit of the PV module can be derived as shown in Figure 6. The PV module consists of several PV cells and two parasitic resistances (R_S , R_P), where each PV cell has a combined structure of an ideal current source (I_p) and a diode (D_p). The current (I_{PV}) of the PV module can be derived as

$$I_{PV} = I_p - I_D - I_{Rp} \quad (1)$$

where $I_p = I_{p1} + I_{p2} \cdots + I_{pn}$ and $I_D = I_{D1} + I_{D2} \cdots + I_{Dn}$. Assuming all PV cells are the same, $I_p = nI_{p1}$ and $I_D = nI_{D1}$ are obtained. Using the Shockley diode equation, I_D is given by

$$I_D = nI_0 \left[e^{(V_{PV} + R_S I_{PV}) / (an_s V_t)} - 1 \right] \quad (2)$$

where n is the number of PV cells connected in parallel, n_s is the number of PV cells connected in series, I_0 is the saturation current of the diode, a is the diode ideality constant, and $V_t = kT/q$ is the thermal voltage of the diode with $q = 1.602 \times 10^{-19}$ C, $k = 1.381 \times 10^{-23}$ J/K, and T is an ambient temperature.

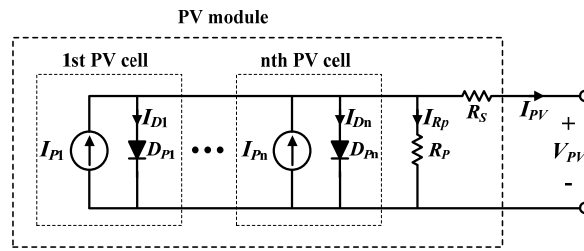


Figure 6. Equivalent circuit of the PV module.

As the voltage across R_p is given by $V_{PV} + R_s I_{PV}$, the current of R_p is obtained as

$$I_{Rp} = \frac{V_{PV} + R_s I_{PV}}{R_p}. \tag{3}$$

Then, inserting (2) and (3) into (1) results in

$$I_{PV} = I_p - nI_0 \left[e^{(V_{PV} + R_s I_{PV}) / (aV_t)} - 1 \right] - \frac{V_{PV} + R_s I_{PV}}{R_p}. \tag{4}$$

Using (4), the characteristic curves of the PV module are drawn as shown in Figure 7. Figure 7a shows the current–voltage characteristic curve of the PV module and Figure 7b shows the power–voltage characteristic curve. These curves have notable variables: short-circuit current (I_{SC}), open-circuit voltage (V_{OC}), maximum power point (MPP), voltage at MPP (V_{MPP}), current at MPP (I_{MPP}), and power at MPP (P_{MPP}).

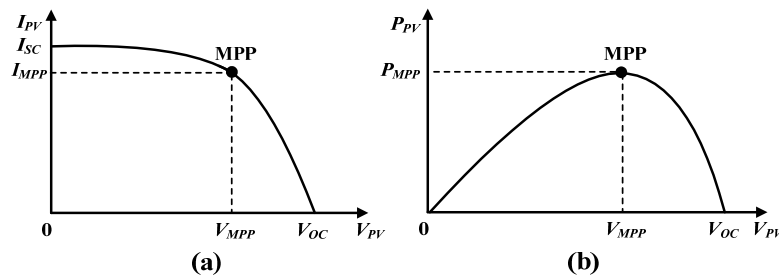


Figure 7. (a) Current–voltage characteristic curve and (b) power–voltage characteristic curve of the PV module.

The current of the PV cell depends on the solar irradiance and the temperature as follows;

$$I_p = n \left[I_{p,STC} + K_I (T - T_n) \right] \frac{G}{G_n} \tag{5}$$

where $I_{p,STC}$ is a light-generated current at the standard test condition (STC, 25°C and 1000 W/m²), K_I is a temperature coefficient, T_n is a nominal temperature (25°C), G is an irradiation level of the PV module, and G_n is a nominal irradiance level (1000 W/m²). Using (5), Equation (4) can be represented as

$$I_{PV} = n \left[I_{p,STC} + K_I (T - T_n) \right] \frac{G}{G_n} - nI_0 \left[e^{(V_{PV} + R_s I_{PV}) / (aV_t)} - 1 \right] - \frac{V_{PV} + R_s I_{PV}}{R_p}. \tag{6}$$

Equation (6) shows that the characteristic curve of the PV module can be changed according to the solar irradiance level and the temperature.

2.1.2. Module-Level Power Electronics (MLPE)

As shown in Figure 8, the MLPE is classified into a micro-inverter and a DC-optimizer. The micro-inverter consists of a DC–DC converter with high voltage gain and a DC–AC inverter, and

the DC-optimizer has only one DC–DC converter with high voltage gain. Therefore, the DC-optimizer can cost less than the micro-inverter, but it needs a DC–AC inverter with high power capability. In the micro-inverter and the DC-optimizer, one MPPT algorithm is applied to each DC–DC converter to optimize each PV module. Therefore, the MPPT algorithms used in the MLPs are called a module-level MPPT, or DMPPT.

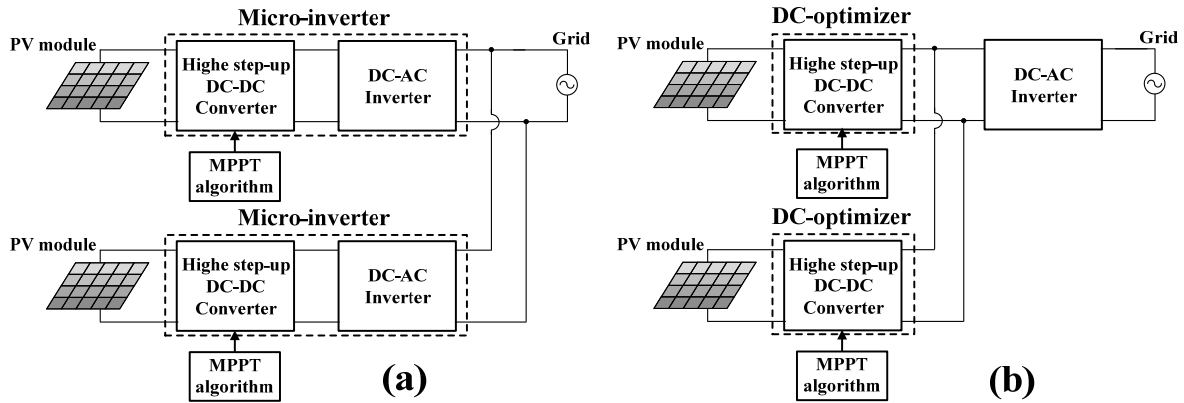


Figure 8. Diagrams of (a) the micro-inverter and (b) the direct current (DC)-optimizer.

2.2. Prosoped MPPT Algorithm

2.2.1. Principle of the Algorithm

The proposed MPPT algorithm uses two methods that can apply the optimal step size to each operating range. In the operating range far from the MPP (non-MPP region), a variable step size ($=k_1 \cdot S \cdot V_{step}$) is automatically adjusted according to the slope of $\Delta P_{PV} / \Delta V_{PV}$ for fast dynamic response. Here, k_1 is a constant coefficient for variable step size, S is a slope coefficient calculated as $|\Delta P_{PV} / \Delta V_{PV}|$, and V_{step} is a fixed step size. In the operating range near the MPP (MPP region), a small fixed step size ($=k_2 \cdot V_{step}$) is used to minimize the oscillations at the MPP, where k_2 is a constant coefficient for small fixed step size.

As shown in Figure 9, the proposed MPPT algorithm has two operating regions including the MPP ($P_{PV} > \beta \cdot P_{MPP}$) and non-MPP ($P_{PV} < \beta \cdot P_{MPP}$) regions, where β is an MPP region coefficient. The operating point starts at $V_{PV} = V_{OC}$ and move with fast tracking speed toward the MPP (V_{MPP}, P_{MPP}). The direction of the operating point is determined using ΔP_{PV} and ΔV_{PV} , where Δ means the difference between the present and previous values. In addition, the present P_{PV} is compared with P_{MPP} to search the MPP.

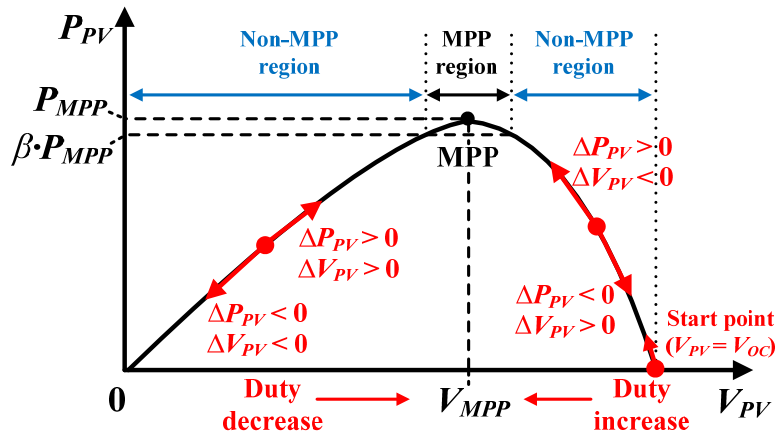


Figure 9. Principle of operation for the proposed MPPT algorithm.

2.2.2. Flow Chart

The flow chart of the proposed MPPT algorithm is shown in Figure 10, and it is described as follows:

1. The present V_{PV} and I_{PV} of the PV module are used as the input signals for the proposed MPPT algorithm. The variable “Flag_start” is preset to 1 for fast tracking speed at the starting point of $V_{PV} = V_{OC}$, and the variable “Flag_reset” is preset to 1 for setting the P_{MPP} and V_{MPP} to the present P_{PV} and V_{PV} , where $P_{PV} = V_{PV} \cdot I_{PV}$.
2. If Flag_start is 1, it is determined that the operating point is located at the starting point of $V_{PV} = V_{OC}$. Therefore, the reference variable (V_{ref}) is initially set to $1/V_{PV}$ ($=1/V_{OC}$) and the operating point moves rapidly toward the MPP. After that, Flag_start is set to 0.
3. In this process, P_{PV} is calculated as $V_{PV} \cdot I_{PV}$, ΔP_{PV} and ΔV_{PV} are calculated using present (P_{PV} and V_{PV}) and previous (P_{PV_b} and V_{PV_b}) values, and the slope coefficient (S) is calculated as $|\Delta P_{PV}/\Delta V_{PV}|$.
4. If Flag_reset is 1, P_{MPP} and V_{MPP} are set to the present P_{PV} and V_{PV} , and then Flag_reset is set to 0.
5. If the present P_{PV} is higher than P_{MPP} , it is determined that the MPP has not been found yet. Therefore, the operating point is forced to keep moving toward the MPP, and P_{MPP} and V_{MPP} are reset to the present P_{PV} and V_{PV} . To quickly find the MPP, the variable step size ($=k_1 \cdot S \cdot V_{step}$) is used in this process.
6. If the operating point is located in the MPP region, the small fixed step size ($=k_2 \cdot V_{step}$) is used to track the MPP accurately.
7. If P_{PV} is lower than the boundary value ($\beta \cdot P_{MPP}$) between the MPP and non-MPP regions, it is determined that the operating point is located in non-MPP region. This process is usually performed under dynamic weather conditions because the MPP changes under these conditions. Therefore, Flag_reset is set to 1 to find a new MPP, and the variable step size ($=k_1 \cdot S \cdot V_{step}$) is automatically adjusted according to the slope of $\Delta P_{PV}/\Delta V_{PV}$ for a fast dynamic response.
8. V_{ref} is limited by the maximum and minimum values ($V_{ref,max}$ and $V_{ref,min}$) of V_{ref} to prevent malfunction of the DC–DC converter in the MLPEs.
9. Through the above processes, a new V_{ref} is obtained. V_{ref} is compared with the carrier signal ($V_{carrier}$) in the digital signal processor (DSP), and a new duty ratio (D) is generated to control the DC–DC converter in the MLPE (Figure 11). In addition, the previous values (P_{PV_b} and V_{PV_b}) are obtained at this time.

The above processes from (1) to (9) are repeated to operate the DC–DC converter at the MPP of the PV module.

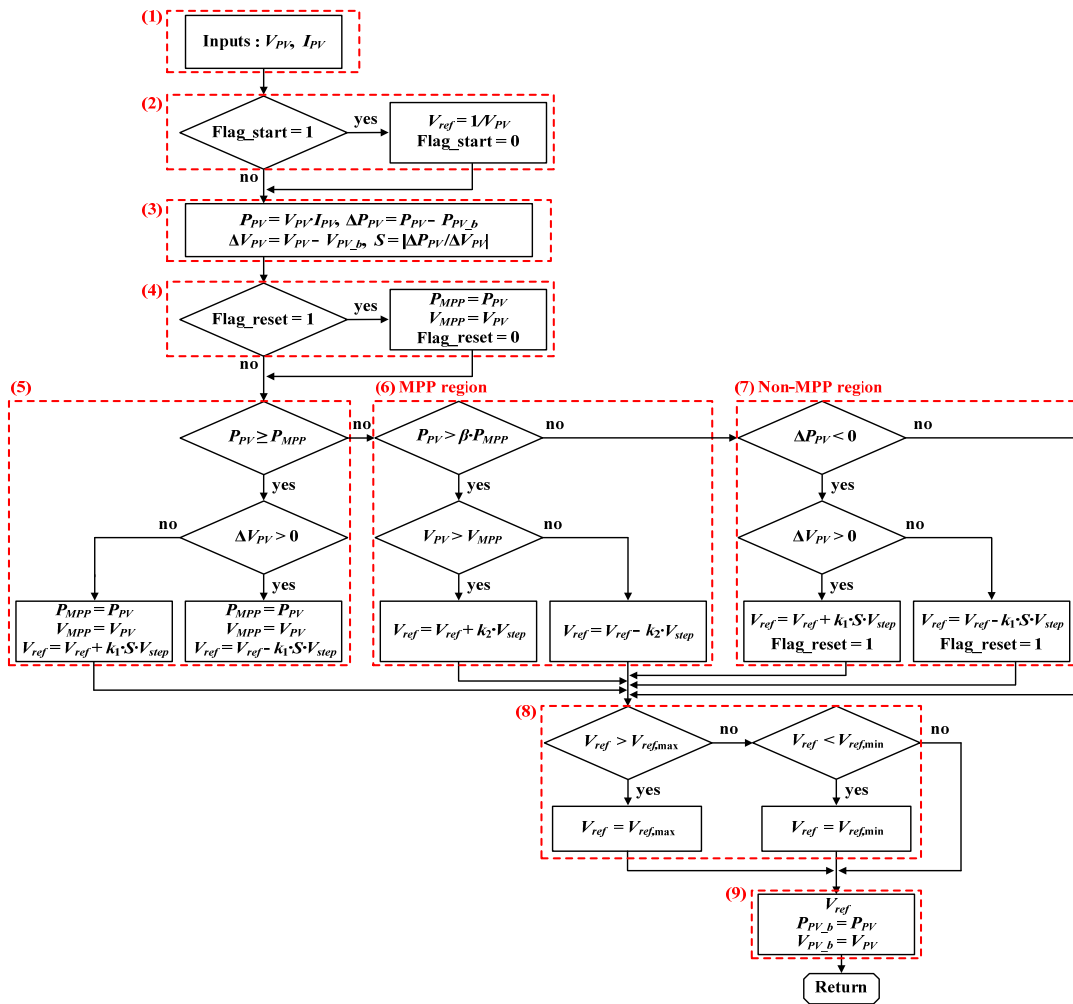


Figure 10. Flow chart of the proposed MPPT algorithm.

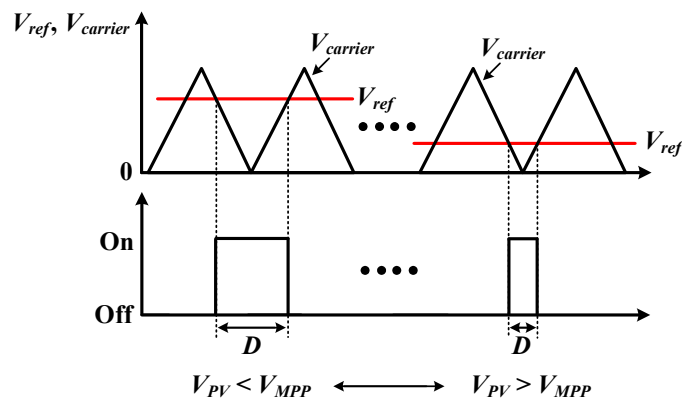


Figure 11. The process for generating a duty ratio (D) in the digital signal processor (DSP).

2.2.3. Design Considerations

- (1) maximum ($V_{ref,max}$) and minimum ($V_{ref,min}$) of V_{ref}

The DC–DC converter in the MLPEs has an input voltage range of $V_{PV,min} \leq V_{PV} \leq V_{PV,max}$ due to its limited voltage gain. Since V_{ref} is calculated as $1/V_{PV}$, $V_{ref,max}$ and $V_{ref,min}$ can be defined as $1/V_{PV,min}$ and $1/V_{PV,max}$, respectively.

- (2) Coefficient (k_1) for variable step size and coefficient (k_2) for small fixed step size

The proposed MPPT algorithm uses a variable step size ($=k_1 \cdot S \cdot V_{step}$) for fast dynamic response in operating range far from the MPP and a small fixed step size ($=k_2 \cdot V_{step}$) for small oscillations in operating range near the MPP, where k_1 , k_2 , and V_{step} have constant values. Due to the fact that the slope coefficient (S) is calculated as $|\Delta P_{PV}/\Delta V_{PV}|$, the variation of the reference variable (V_{ref}) is given by

$$|\Delta V_{ref}| = k_1 \left| \frac{\Delta P_{PV}}{\Delta V_{PV}} \right| V_{step} \quad (7)$$

where Δ means a difference between the present and previous values. The operating point of the proposed MPPT algorithm reaches the MPP ($V_{PV} = V_{MPP}$, $P_{PV} = P_{MPP}$) after starting at the point ($V_{PV} = V_{OC}$, $P_{PV} = 0$), where V_{OC} is an open-circuit voltage of the PV module. Considering only the starting point and the MPP at the STC (25 °C and 1000 W/m²), the above equation can be represented using $V_{ref} = 1/V_{PV}$ as

$$\frac{1}{V_{MPP,STC}} - \frac{1}{V_{OC}} = k_1 \frac{P_{MPP,STC}}{V_{OC} - V_{MPP,STC}} V_{step} \quad (8)$$

where $V_{MPP,STC}$ and $P_{MPP,STC}$ are the voltage and power at the MPP under the STC (25 °C and 1000 W/m²).

Therefore, k_1 can be obtained as

$$k_1 = \frac{(V_{OC} - V_{MPP,STC})^2}{V_{OC} V_{MPP,STC} V_{step} P_{MPP,STC}} \quad (9)$$

The small step coefficient (k_2) can be determined by considering the resolution of V_{PV} in the operating range near the MPP. If accuracy of the third decimal point of V_{PV} is required in operating range near the MPP, $|\Delta V_{ref}| = k_2 \cdot V_{step}$ can be represented using $V_{ref} = 1/V_{PV}$ as

$$\frac{1}{V_{MPP,STC}} - \frac{1}{V_{MPP,STC} + 0.001} = k_2 V_{step} \quad (10)$$

Therefore, k_2 is calculated as

$$k_2 = \frac{0.001}{V_{MPP,STC} (V_{MPP,STC} + 0.001) V_{step}} \quad (11)$$

(3) MPP region coefficient (β)

$\beta \cdot P_{MPP}$ is a boundary value between the MPP and non-MPP regions. For fast dynamic response, β should be close to one; however, if it is too close to one, oscillations can occur at the boundary of $P_{PV} = \beta \cdot P_{MPP}$. Therefore, $\beta = 0.9 \sim 0.95$ is recommended.

(4) Fixed step size (V_{step})

To optimize the proposed MPPT algorithm in a given DC–DC converter topology and operating conditions, V_{step} is determined after several experiments. Therefore, V_{step} has a user-defined value, and $V_{step} = 10$ was used for the experiments in this paper.

3. Experimental Results and Discussion

3.1. Experimental Results

Figure 12 shows the equipment settings to evaluate the performances of the MPPT algorithms. The output cable of the PV simulator (ETS60 from AMETEK Inc.) is connected to the input of the DC–DC converter (boost half-bridge topology), and the LAN cable of the PV simulator is connected to the notebook computer to set the characteristic curve (Figure 13) of the commercial 300-W PV module (Q.PEAK-G4.1 300 from Hanwha Inc.). Here, according to the irradiance level (E) and the module

temperature (T), the electrical characteristics of the PV module “Q.PEAK-G4.1 300” are listed in Table 4. The output of the DC–DC converter is connected to the electronic load (DL1000H from NF Corp.) to consume the energy, and the notebook computer is connected to the DSP (TMS320F28335 from Texas Instruments Inc.) in the DC–DC converter by USB cable. The power meter (PW3336, from HIOKI Inc.) is used to measure the voltage (V_{PV}), current (I_{PV}), and power (P_{PV}) of the PV simulator. Based on the sensed V_{PV} and I_{PV} , the DSP runs the MPPT algorithm and generates the gate signals (v_{gs1} , v_{gs2}) for operating the DC–DC converter. To compare the dynamic and energy utilization performances of the MPPT algorithms, four experiments were performed as follows.

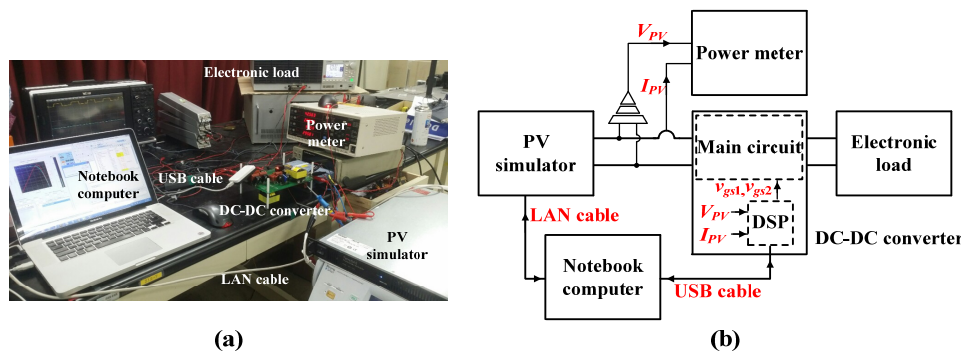


Figure 12. (a) Photograph and (b) block diagram of the equipment settings for experiments to evaluate the MPPT performance.

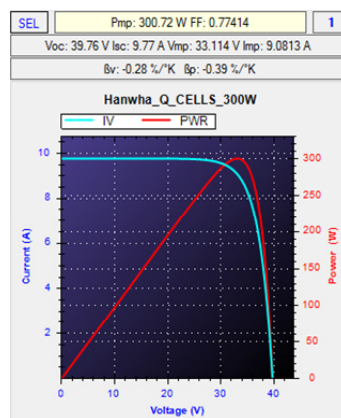


Figure 13. Electrical characteristic curve of a 300 W PV module “Q.PEAK-G4.1 300” under the standard test conditions (STC) of irradiance level of 1000 W/m² and module temperature of 25 °C.

Table 4. Electrical characteristics of the PV module “Q.PEAK-G4.1 300” at different irradiance levels (E) and module temperatures (T).

Conditions	Open-Circuit Voltage (V_{OC})	Short-Circuit Current (I_{SC})	Voltage at MPP (V_{MPP})	Current at MPP (I_{MPP})	Power at MPP (P_{MPP})
E = 1000 W/m ² and T = 25 °C	39.76 V	9.77 A	33.11 V	9.082 A	300.71 W
E = 100 W/m ² and T = 25 °C	35.78 V	1.086 A	29.8 V	1.009 A	30.07 W
E = 700 W/m ² and T = 15 °C	40.24 V	7.021 A	33.51 V	6.527 A	218.72 W
E = 700 W/m ² and T = 75 °C	33.66 V	6.502 A	28.04 V	6.044 A	169.47 W

First, the proposed MPPT algorithm and the conventional MPPT algorithms including a basic P&O of [21], an adaptive P&O of [26], and an adaptive INC of [27] were tested at the STC of E = 1000 W/m² and T = 25 °C. Figure 14 shows the measured V_{PV} , I_{PV} , and P_{PV} waveforms of the PV module when each MPPT algorithm is applied to a DC–DC converter. The basic P&O algorithm with a small fixed step size tracked the maximum power point (MPP) slowly, but it had small oscillations after reaching

the MPP (Figure 14a). When the fixed step size increased, the tracking speed of the basic P&O algorithm increased as well, but the oscillations also increased (Figure 14b). To solve the problem of the fixed step size, the adaptive P&O and adaptive INC algorithms used a variable step size proportional to $k_1 \cdot \Delta P_{PV} / \Delta V_{PV}$. However, these algorithms still had the oscillations at the MPP because the $\Delta P_{PV} / \Delta V_{PV}$ is easily affected by sensing and calculation errors, sensing noise, and the ripples of V_{PV} and I_{PV} (Figure 14c–f). If the coefficient k_1 is smaller, the oscillations at the MPP decreases, but the tracking speed is slower. To improve the problems of the previous MPPT algorithms mentioned above, the proposed MPPT algorithm uses two methods that can apply the optimal step size to each operating range. In the operating range near the MPP, a small fixed step size is used to minimize the oscillations at the MPP, but in the operating range far from the MPP, a variable step size proportional to $k_1 \cdot \Delta P_{PV} / \Delta V_{PV}$ is used to achieve fast tracking speed. The proposed MPPT algorithm can adjust the tracking speed using k_1 so that it can track the MPP quickly. As a result, the proposed MPPT algorithm tracked the MPP with faster tracking speed and had smaller oscillations at the MPP when compared with the conventional algorithms (Figure 14g,h).

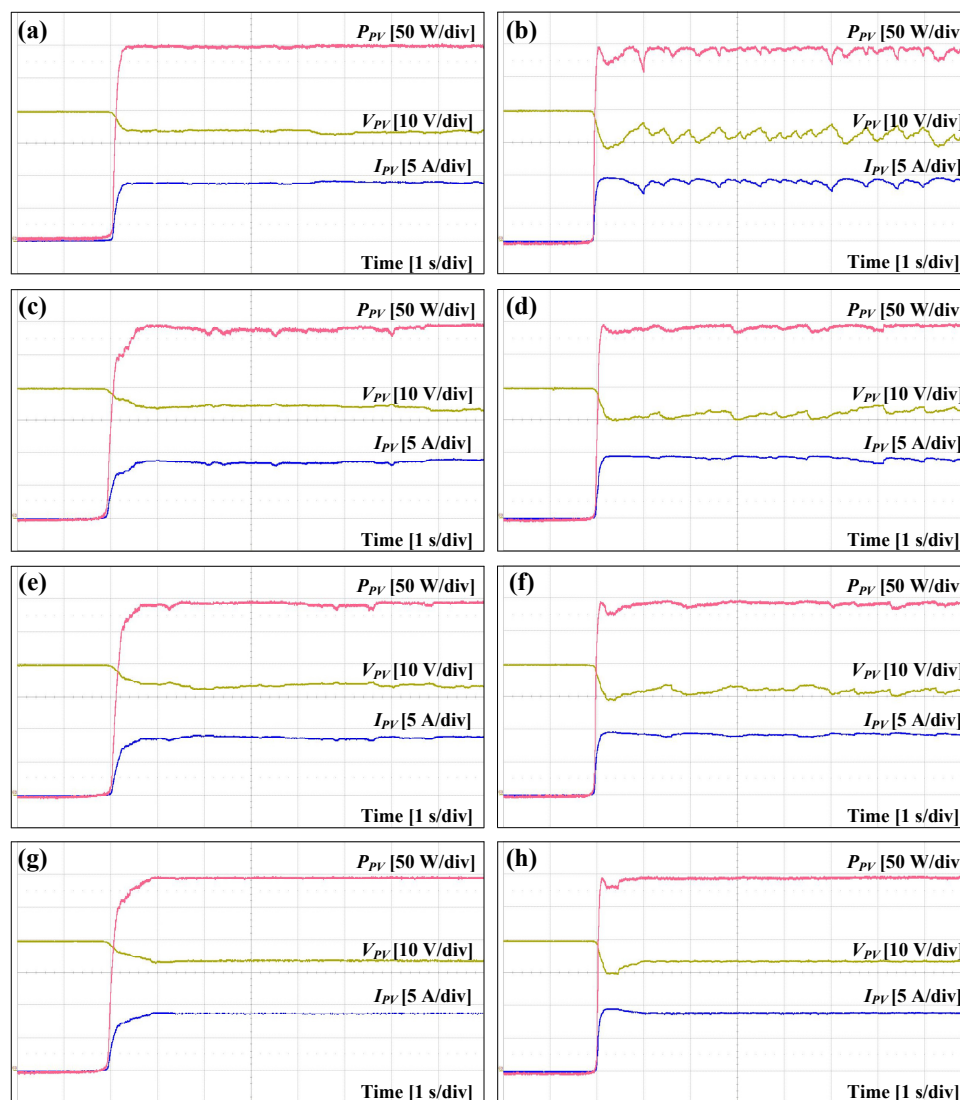


Figure 14. Voltage (V_{PV}), current (I_{PV}), and power (P_{PV}) waveforms of the PV module measured using the basic P&O algorithm with (a) small fixed step size or (b) large fixed step size, using the adaptive P&O algorithm with (c) low k_1 ($=0.00002$) or (d) high k_1 ($=0.0001$), using the adaptive INC algorithm with (e) low k_1 ($=0.00002$) or (f) high k_1 ($=0.0001$), and using the proposed MPPT algorithm with (g) low k_1 ($=0.00002$) and small fixed step size or (h) high k_1 ($=0.0001$) and small fixed step size.

The MPPT efficiencies of the proposed and conventional MPPT algorithms were measured for two minutes after reaching the MPP under the same conditions as in Figure 14 (Figure 15). When a large fixed step size was applied, the basic P&O algorithm had the lowest average MPPT efficiency of 97.8% due to the largest oscillations at the MPP (Figure 15a). The adaptive P&O and adaptive INC algorithms with high k_1 (=0.0001) had higher average MPPT efficiencies of 98.5% and 98.7% than that of the basic P&O algorithm because they used variable step sizes (Figure 15b,c). In addition, the adaptive P&O and adaptive INC algorithms had higher average MPPT efficiencies of 99.1% and 98.9% than 98.7% of the basic P&O algorithm when small fixed step size and low k_1 (=0.00002) were applied. The proposed MPPT algorithm had the highest average MPPT efficiencies of 99.4% and 99.7% at low k_1 (=0.00002) and high k_1 (=0.0001) because it had the smallest oscillations at the MPP (Figure 15d).

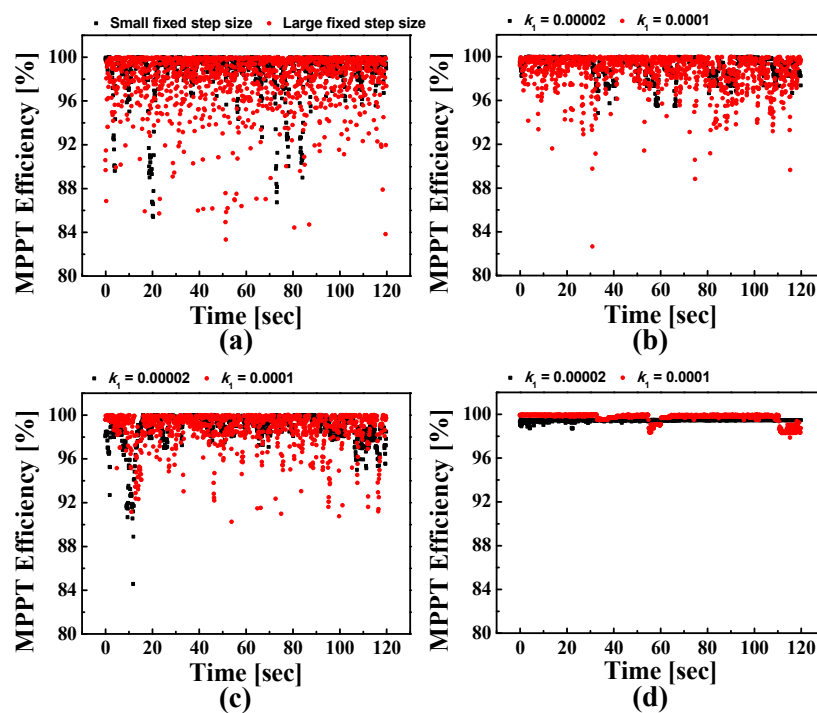


Figure 15. Measured MPPT efficiencies of (a) the basic P&O with small or large fixed step sizes, (b) the adaptive P&O with low k_1 (=0.00002) or high k_1 (=0.0001), (c) the adaptive INC with low k_1 (=0.00002) or high k_1 (=0.0001), and (d) the proposed MPPT algorithms with low k_1 (=0.00002) or high k_1 (=0.0001).

The P_{PV} waveforms were measured to compare the performances of the proposed and conventional MPPT algorithms when irradiance level changed abruptly from 1000 W/m² to 100 W/m² or from 100 W/m² to 1000 W/m² at a constant temperature of 25 °C (Figure 16). In each MPPT algorithm, the fixed step size and k_1 were optimized by considering the trade-off between the tracking speed and the oscillations under the given conditions. When irradiance level changed from 100 W/m² to 1000 W/m², the basic P&O algorithm tracked the MPP within 20 s but had large oscillations (Figure 16a). The adaptive P&O and adaptive INC algorithms also tracked the MPP within 20 s, but they still had oscillations (Figure 16b,c). As shown in Figure 14c–f, these algorithms could reduce the oscillations using a small fixed step size or k_1 , but the tracking was slower. The proposed MPPT algorithm had no trade-off between the tracking speed and the oscillations because it uses a variable step size proportional to $k_1 \cdot \Delta P_{PV} / \Delta V_{PV}$ in the operating range far from the MPP and a small fixed step size in the operating range near the MPP. Therefore, when the irradiance level changed from 100 W/m² to 1000 W/m², the proposed MPPT algorithm showed smaller oscillations and faster tracking speed than other algorithms (Figure 16d).

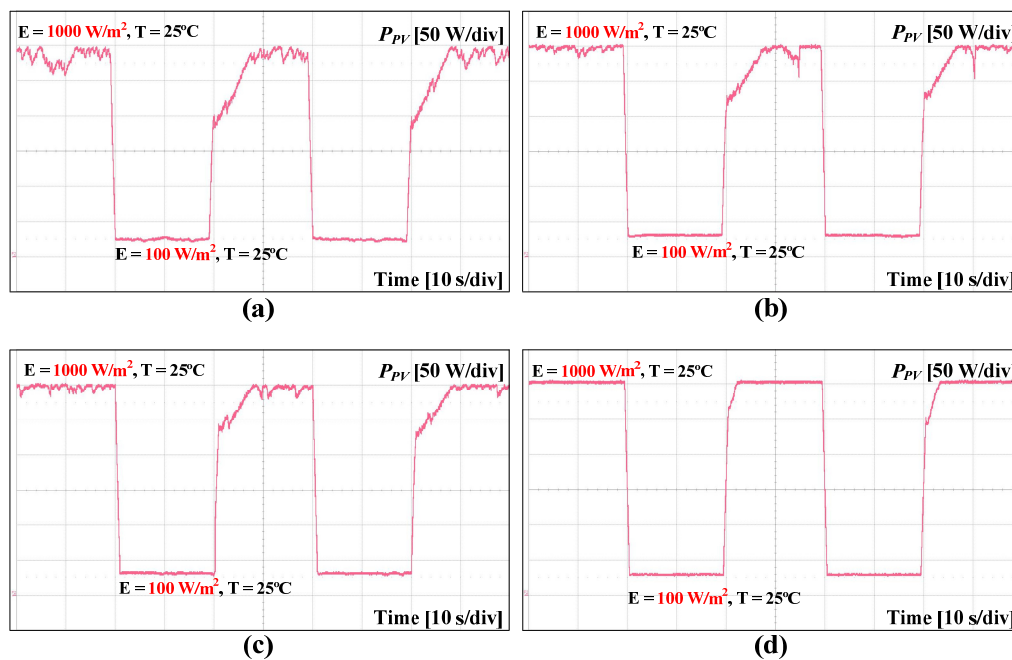


Figure 16. Power (P_{PV}) waveforms of the PV module measured using (a) the basic P&O algorithm, (b) the adaptive P&O algorithm, (c) the adaptive INC algorithm, and (d) the proposed MPPT algorithm under abruptly changing irradiance conditions.

Figure 17 shows the P_{PV} waveforms measured to compare the performances of the proposed and conventional MPPT algorithms when the temperature changed abruptly from 15 °C to 75 °C or from 75 °C to 15 °C at a constant irradiance of 700 W/m². In each MPPT algorithm, the fixed step size and k_1 were optimized by considering the trade-off between the tracking speed and the oscillations under the given conditions. The basic P&O algorithm slowly tracked the MPP due to the fixed step size when the temperature changed from 75 °C to 15 °C (Figure 17a). The adaptive P&O and adaptive INC algorithms tracked the MPP faster than the basic P&O, but they still had oscillations after reaching the MPP (Figure 17b,c). The proposed MPPT algorithm not only had the fastest tracking speed but also had the smallest oscillations after reaching the MPP because it had no trade-off between the tracking speed and the oscillations (Figure 17d). The above results of the comparison experiments are summarized in Table 5.

3.2. Discussion

Among many MPPT algorithms, the P&O method was widely used due to its simple principle and ease of implementation. However, the basic P&O algorithm of [21] had a trade-off between tracking speed and oscillations due to a fixed step size (Figure 14a,b). To solve this problem, the adaptive P&O and adaptive INC algorithms using a variable step size were introduced [26,27]. These adaptive MPPT algorithms can reduce the oscillations at the MPP because the variable step size is automatically adjusted according to the slope ($\Delta P_{PV}/\Delta V_{PV}$) of the P–V curve (Figure 14c–f). However, the adaptive MPPT algorithms still had oscillations after reaching the MPP because the calculated $\Delta P_{PV}/\Delta V_{PV}$ is easily affected by sensing and calculation errors, sensing noise, and the ripples of V_{PV} and I_{PV} . To improve the performances of the conventional MPPT algorithms mentioned above, the proposed MPPT algorithm used a small fixed step size in operating range near the MPP and a variable step size proportional to $k_1 \cdot \Delta P_{PV}/\Delta V_{PV}$ in operating range far from the MPP. As a result, the proposed MPPT algorithm had higher MPPT efficiency than the conventional MPPT algorithms (Figure 15) and showed faster tracking speed and smaller oscillations under dynamic weather conditions (Figures 16 and 17). These advantages of the proposed MPPT algorithm enable the distributed PV system to operate at its maximum performance, regardless of weather conditions.

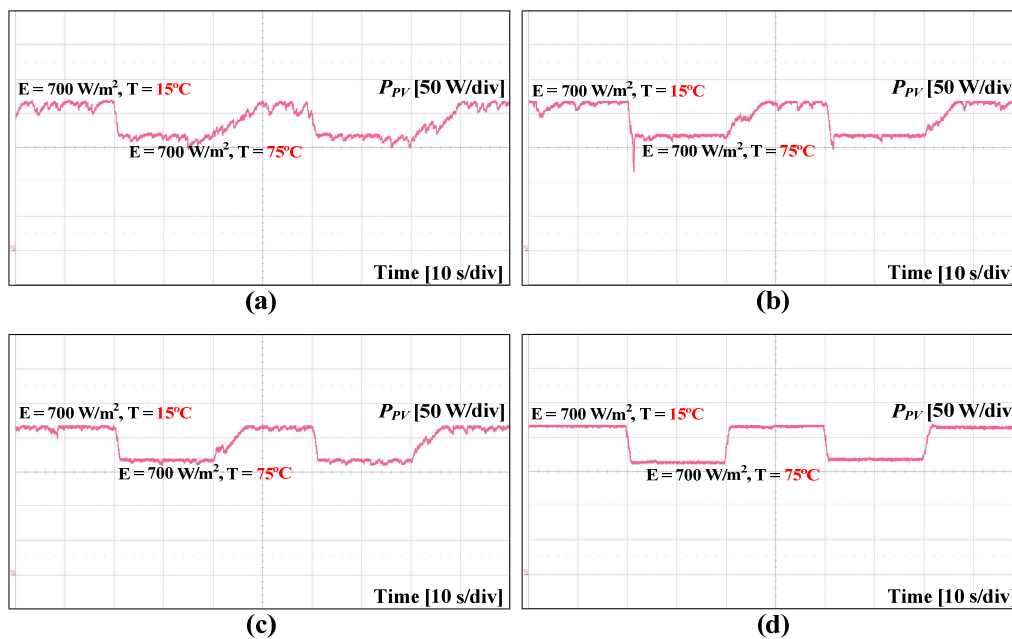


Figure 17. Power (P_{PV}) waveforms of the PV module measured using (a) the basic P&O algorithm, (b) the adaptive P&O algorithm, (c) the adaptive INC algorithm, and (d) the proposed MPPT algorithm under abruptly changing temperature conditions.

Table 5. Comparisons between the proposed and conventional MPPT algorithms.

Performance Parameters	Basic P&O Algorithm of [21]	Adaptive P&O Algorithm of [26]	Adaptive INC Algorithm of [27]	Proposed Algorithm
Implementation complexity	simple	medium	medium	medium
MPPT method	fixed step size ($k_2 V_{step}$) in whole operating range	variable step size ($k_1 V_{step} \Delta P_{PV} / \Delta V_{PV}$) in whole operating range	variable step size ($k_1 V_{step} \Delta P_{PV} / \Delta V_{PV}$) in whole operating range	small fixed step size ($k_2 V_{step}$) near the MPP, variable step size ($k_1 V_{step} \Delta P_{PV} / \Delta V_{PV}$) far from the MPP
MPPT efficiency	97.8%	98.5%	98.7%	99.7%
Performance at rapid change of irradiance	poor	medium	medium	good
Performance at rapid change of temperature	poor	medium	medium	good
Speed	fast	fast	fast	fast
Accuracy	low	medium	medium	high

4. Conclusions

In this paper, an advanced MPPT algorithm for distributed PV systems was proposed. The proposed MPPT algorithm improved the MPPT accuracy and dynamic response of the conventional MPPT algorithms by using two methods that can apply the optimal step size to each operating range. In the operating range near the MPP, a small fixed step size is used to minimize the oscillations at the MPP, but in the operating range far from the MPP, a variable step size proportional to $k_1 \cdot \Delta P_{PV} / \Delta V_{PV}$ is used to achieve fast tracking speed. These advantages of the proposed MPPT algorithm were verified by comparison with the conventional MPPT algorithms: a basic P&O algorithm with fixed step size,

an adaptive P&O algorithm with variable step size, and an adaptive INC algorithm with a variable step size. In the experimental results, the proposed MPPT algorithm had the highest MPPT efficiency of 99.7% compared with the conventional MPPT algorithms. In addition, it showed the fastest tracking speed and smallest oscillations under abruptly changing irradiance levels and temperature conditions. Due to these advantages of the proposed MPPT algorithm, the PV systems using the proposed MPPT algorithm can produce more electrical energy than that using the conventional MPPT algorithms. Moreover, the proposed MPPT algorithm requires low computational load of DSP because the formulas used for step size are simple, which is a good advantage in terms of user convenience and cost that are important for commercialization. As a result, the proposed MPPT algorithm is well-suited for distributed PV systems requiring high MPPT efficiency and fast dynamic response.

Author Contributions: Both authors contributed equally to this work. H.-S.L. presented the main idea of the MPPT algorithm. H.-S.L. and J.-J.Y. analyzed the proposed MPPT algorithm and performed experiments. J.-J.Y. contributed to the overall composition and writing of the manuscript.

Funding: This work was supported by the National Research Foundation of Korea (NRF) grant funded by the government of Korea (MSIP) (NRF-2018R1A1A1A05079496). This research was also supported by the Korea Electric Power Corporation (Grant number: R17XA05-15).

Conflicts of Interest: The authors have no conflict of interest.

References

1. Malinowski, M.; Leon, J.I.; Abu-Rub, H. Solar photovoltaic and thermal energy systems: Current technology and future trends. *Proc. IEEE* **2017**, *105*, 2132–2146. [[CrossRef](#)]
2. Kroposki, B.; Johnson, B.; Zhang, Y.; Gevorgian, V.; Denholm, P.; Hodge, B.M.; Hannegan, B. Achieving a 100% renewable grid: Operating electric power systems with extremely high levels of variable renewable energy. *IEEE Power Energy Mag.* **2017**, *15*, 61–73. [[CrossRef](#)]
3. García-Rodríguez, L. Renewable Energy Applications in Desalination: State of the Art. *Sol. Energy* **2003**, *75*, 381–393. [[CrossRef](#)]
4. Renewables 2019 Global Status Report, Renewable Energy Policy Network for the 21st Century (REN21). 2019. Available online: <https://www.ren21.net/gsr-2019/> (accessed on 2 September 2019).
5. Romero-Cadaval, E.; Francois, B.; Malinowski, M.; Zhong, Q.C. Grid-connected photovoltaic plants: An alternative energy source, replacing conventional sources. *IEEE Ind. Electron. Mag.* **2015**, *9*, 18–32. [[CrossRef](#)]
6. Zhao, P.; Suryanarayanan, S.; Simoes, M.G. An energy management system for building structures using a multi-agent decision-making control methodology. *IEEE Trans. Ind. Appl.* **2013**, *49*, 322–330. [[CrossRef](#)]
7. Strunz, K.; Abbasi, E.; Huu, D.N. DC microgrid for wind and solar power integration. *IEEE J. Emerg. Sel. Top. Power Electron.* **2014**, *2*, 115–126. [[CrossRef](#)]
8. Feldman, D.; Barbose, G.; Margolis, R.; Bolinger, M.; Chung, D.; Fu, R.; Seel, J.; Davidson, C.; Darghouth, N.; Wiser, R. Photovoltaic System Pricing Trends Historical, Recent, and Near-Term Projections 2015 Edition. Available online: <https://escholarship.org/content/qt9pc3x32t/qt9pc3x32t.pdf> (accessed on 2 September 2019).
9. Zsiborács, H.; Hegedűsné Baranyai, N.; Csányi, S.; Vincze, A.; Pintér, G. Economic Analysis of Grid-Connected PV System Regulations: A Hungarian Case Study. *Electronics* **2019**, *8*, 149. [[CrossRef](#)]
10. Camera, F.L. *Renewable Power Generation Costs in 2018*; International Renewable Energy Agency (IRENA): Abu Dhabi, UAE, 2019. Available online: <https://www.irena.org/publications/2019/May/Renewable-power-generation-costs-in-2018> (accessed on 2 September 2019).
11. Meza, C.; Negroni, J.J.; Biel, D.; Guinjoan, F. Energy-balance modeling and discrete control for single-phase grid-connected PV central inverters. *IEEE Trans. Ind. Electron.* **2008**, *55*, 2734–2743. [[CrossRef](#)]
12. Flicker, J.; Tamizhmani, G.; Moorthy, M.K.; Thiagarajan, R.; Ayyanar, R. Accelerated testing of module-level power electronics for longterm reliability. *IEEE J. Photovolt.* **2017**, *7*, 259–267. [[CrossRef](#)]
13. Liu, Y.H.; Chen, J.H.; Huang, J.W. A review of maximum power point tracking techniques for use in partially shaded conditions. *Renew. Sustain. Energy Rev.* **2015**, *41*, 436–453. [[CrossRef](#)]
14. Gu, B.; Dominic, J.; Lai, J.S.; Zhao, Z.; Liu, C. High boost ratio hybrid transformer DC-DC converter for photovoltaic module applications. *IEEE Trans. Power Electron.* **2013**, *28*, 2048–2058. [[CrossRef](#)]

15. Sinapis, K.; Tzikas, C.; Litjens, G.; Van den Donker, M.; Folkerts, W.; Van Sark, W.G.J.H.M.; Smets, A. A comprehensive study on partial shading response of c-Si modules and yield modeling of string inverter and module level power electronics. *Sol. Energy* **2016**, *135*, 731–741. [[CrossRef](#)]
16. Aganza-Torres, A.; Cardenas, V.; Pacas, M.; Gonzales, M. An efficiency comparative analysis of isolated multi-source grid-connected PV generation systems based on a HF-link micro-inverter approach. *Sol. Energy* **2016**, *127*, 239–249. [[CrossRef](#)]
17. Luo, H.; Wen, H.; Li, X.; Jiang, L.; Hu, Y. Synchronous buck converter based low-cost and high-efficiency sub-module DMPPT PV system under partial shading conditions. *Energy Convers. Manag.* **2016**, *126*, 473–487. [[CrossRef](#)]
18. Femia, N.; Lisi, G.; Petrone, G.; Spagnuolo, G.; Vitelli, M. Distributed maximum power point tracking of photovoltaic arrays: Novel approach and system analysis. *IEEE Trans. Ind. Electron.* **2008**, *55*, 2610–2621. [[CrossRef](#)]
19. Wang, F.; Fang, Z.; Lee, F.C.; Zhu, T.; Yi, H. Analysis of existence-judging criteria for optimal power regions in DMPPT PV systems. *IEEE Trans. Energy Convers.* **2016**, *31*, 1433–1441. [[CrossRef](#)]
20. Ahmed, A.; Ran, L.; Bumby, J. Perturbation parameters design for hill climbing MPPT techniques. In Proceedings of the IEEE International Symposium on Industrial Electronics, Hangzhou, China, 28–31 May 2012. [[CrossRef](#)]
21. Hua, C.; Lin, J.; Shen, C. Implementation of a DSP-controlled photovoltaic system with peak power tracking. *IEEE Trans. Ind. Electron.* **1998**, *45*, 99–107. [[CrossRef](#)]
22. Veerachary, M.; Senjyu, T.; Uezato, K. Voltage-based maximum power point tracking control of PV system. *IEEE Trans. Aerosp. Electron. Syst.* **2002**, *38*, 262–270. [[CrossRef](#)]
23. Femia, N.; Petrone, G.; Spagnuolo, G.; Vitelli, M. Optimization of perturb and observe maximum power point tracking method. *IEEE Trans. Power Electron.* **2005**, *20*, 963–973. [[CrossRef](#)]
24. Safari, A.; Mekhilef, S. Simulation and hardware implementation of incremental conductance MPPT with direct control method using cuk converter. *IEEE Trans. Ind. Electron.* **2011**, *58*, 1154–1161. [[CrossRef](#)]
25. Xiao, W.; Dunford, W.G. A modified adaptive hill climbing MPPT method for photovoltaic power systems. In Proceedings of the IEEE 35th Annual Power Electronics Specialists Conference, Aachen, Germany, 20–25 June 2004. [[CrossRef](#)]
26. Zhang, X.; Zhang, H.; Zhang, H.; Zhang, P.; Wang, F.; Jia, H.; Song, D. A variable step-size P&O method in the application of MPPT control for a PV system. In Proceedings of the IEEE Advanced Information Management, Communicates, Electronic and Automation Control Conference (IMCEC), Xi'an, China, 3–5 October 2016. [[CrossRef](#)]
27. Liu, F.; Duan, S.; Liu, F.; Liu, B.; Kang, Y. A variable step size INC MPPT method for PV systems. *IEEE Trans. Ind. Electron.* **2008**, *55*, 2622–2628. [[CrossRef](#)]
28. Pandey, A.; Dasgupta, N.; Mukerjee, A.K. High-performance algorithms for drift avoidance and fast tracking in solar MPPT system. *IEEE Trans. Energy Convers.* **2008**, *23*, 681–689. [[CrossRef](#)]
29. Aashoor, F.A.O.; Robinson, F.V.P. A Variable Step Size Perturb and Observe Algorithm for Photovoltaic Maximum Power Point Tracking. In Proceedings of the 47th International Universities Power Engineering Conference (UPEC), London, UK, 4–7 September 2012. [[CrossRef](#)]
30. Macaulay, J.; Zhou, Z. A fuzzy logical-based variable step size P&O MPPT algorithm for photovoltaic system. *Energies* **2018**, *11*, 1340. [[CrossRef](#)]
31. Chen, Y.T.; Jhang, Y.C.; Liang, R.H. A fuzzy-logic based auto-scaling variable step-size MPPT method for PV systems. *Sol. Energy* **2016**, *126*, 53–63. [[CrossRef](#)]
32. Harrag, A.; Messalti, S. Variable step size modified p&o mppt algorithm using ga-based hybrid offline/online pid controller. *Renew. Sustain. Energy Rev.* **2015**, *49*, 1247–1260. [[CrossRef](#)]
33. Villalva, M.G.; Gazoli, J.R.; Filho, E.R. Comprehensive approach to modeling and simulation of photovoltaic arrays. *IEEE Trans. Power Electron.* **2009**, *24*, 1198–1208. [[CrossRef](#)]
34. Shongwe, S.; Hanif, M. Comparative analysis of different singlediode PV modeling methods. *IEEE J. Photovolt.* **2015**, *5*, 938–946. [[CrossRef](#)]

